Influence of sustained loading on fracture properties of concrete

Dong, Wei; Zhang, Xue; Zhang, BinSheng; Wu, Qiao

DOI:
10.1016/j.engfracmech.2018.07.034

Publication date:
2018

Influence of sustained loading on fracture properties of concrete

Wei Dong[1,*], Xue Zhang[2], BinSheng Zhang[3], Qiao Wu[4]

[1]Associate Professor, State Key Laboratory of Coastal and Offshore Engineering, Dalian University of Technology, Dalian 116024, P. R. China. E-mail: dongwei@dlut.edu.cn

*Corresponding author

[2]Lecturer, State Key Laboratory of Coastal and Offshore Engineering, Dalian University of Technology, Dalian 116024, P. R. China. E-mail: Xuezhang@dlut.edu.cn

[3]Professor, Department of Construction and Surveying, School of Engineering and Built Environment, Glasgow Caledonian University, Glasgow G4 0BA, Scotland, United Kingdom. E-mail: Ben.Zhang@gcu.ac.uk

[4]Postgratuate student, State Key Laboratory of Coastal and Offshore Engineering, Dalian University of Technology, Dalian 116024, P. R. China. E-mail: 15129485818@mail.dlut.edu.cn

Abstract

To investigate the effects of sustained loading on the fracture properties of concrete, basic creep and three-point bending (TPB) tests were conducted on the pre-notched beams. The specimens were first subjected to two sustained loading levels, i.e. 30% peak load and the initial cracking load over 115 days. Then, they were moved out from the loading frames and tested under TPB loading until failure. The critical crack propagation length (Δa_c), the peak load (P_{max}) and the fracture energy (G_f) were measured in the tests, and the unstable fracture toughness (K_{IC}^{un}) was calculated accordingly. Furthermore, based on the load-displacement curves obtained in the TPB tests, the energy dissipation was derived using the modified J-integral method. By enforcing balance between the energy dissipated and the energy caused by the fictitious cohesive force acting on the fracture process zone, the tension-softening constitutive laws under the two sustained loading levels were established and also simplified as bilinear forms for practical applications. Finally, the effects of sustained loading on the fracture properties were examined by comparing with the tested results from the aging specimens in the static TPB tests. The test results indicate that low sustained loading had no effects on all fracture properties of concrete investigated in this study, while under high sustained loading, Δa_c and K_{IC}^{un} increased and G_f and P_{max} almost remained unchanged. Meanwhile, a smaller free-stress crack opening displacement was obtained under the high sustained loading level, which indicates a shorter FPZ length formed, resulting in the increase in brittleness of concrete.

Keywords: Sustained loading; Concrete; Fracture properties; Tension-softening constitutive law.

Nomenclature

a_0	initial crack length
a_c	critical crack length
a_f	crack propagation length in creep tests
a_{max}	ligament length
B	width of the beam under TPB
$CMOD$	crack mouth opening displacement
$CMOD_c$	critical crack mouth opening displacement
COD	crack opening displacement
$CTOD$	crack tip opening displacement
D	height of the beam under TPB
E	elastic modulus
f_c	uniaxial compressive strength of concrete
f_t	splitting tensile strength of concrete
G_f	fracture energy
δ	loading point displacement
H_0	thickness of the knife edge
K_{IC}^{un}	unstable fracture toughness of concrete
P	applied load
P_{ini}	initial cracking load
P_{max}	peak load
S	span of the beam under TPB
Δa_c	critical crack propagation length
σ	cohesive stress
σ_s	stress corresponding to the break point in the bilinear σ-w relationship
δ	loading-point displacement
δ_0	loading-point displacement corresponding to the peak load
δ_p	residual displacement in a fully unloaded state under TPB
δ_{max}	maximum loading-point displacement
w	crack opening displacement
w_c	residual crack tip opening displacement after unloading in the creep test
w_{ini}	crack opening displacement corresponding to the crack initiation
w_p	crack tip opening displacement before unloading in the creep test
w_{max}	maximum crack opening displacement
w_s	displacement corresponding to the break point in the bilinear σ-w relationship
w_0	stress-free crack width

1. Introduction

In practical engineering, most concrete structures in service are under sustained loading, such as gravity dams, protecting shells in nuclear power stations, cooling towers in thermal power plants, etc. Usually, behaviour of concrete is considered to be viscoelastic under low loading levels [1]. In contrast, cracks initiate, develop and interact with viscoelasticity of concrete under high loading levels, producing high short-term and long-term deformations on concrete structures and largely influencing their load-carrying capacity and durability [2]. Also, the strain of concrete at the crack tip may be large enough to reach its ultimate tensile value, resulting in the initiation and development of new cracks even though the stress level of concrete is below its static tensile strength [3]. It is also possible for existing cracks to propagate unstably when the stress intensity factor (SIF) at the crack tip is even below the fracture toughness [2]. These time-dependent behaviours for concrete are associated with the variations of the cohesive stress in the fracture process zone (FPZ) over time, where the stress relaxation occurs and the released strain energy booms the crack propagation [3, 4]. Hence, the experimental results from static tests cannot be directly used to comprehensively analyse the fracture behaviour of concrete structures under sustained loading. Therefore, it is significant to further explore the fracture properties of concrete under sustained loading so that the crack propagation process and load-carrying capacity of concrete can be predicted more precisely.

In the past decades, many attempts have been made to extensively investigate the time-dependent fracture behaviour of concrete and associate the fracture characteristics of concrete with the time by means of loading rate [5], crack growth rate [6] and long-term loading time [7, 8]. Accordingly, the effects of loading rate on the fracture parameters [5], crack growth rate on the stress intensity curves and long-term load on the deformation [9], failure time [10] and residual loading capacity [11] have been investigated. In the case of sustained loading, it has been widely known that the loading level has a significant effect on the fracture properties of concrete. According to the research by Omar et al. [12], the crack propagation under high sustained loading could reduce the cracking resistance, which is similar to the case of fracture at a slow loading rate. The descending branch of a static load-displacement curve can be regarded as the envelope of the creep fracture curves under high sustained loading, so that the fracture energies under sustained loading and static loading are close to each other [13]. Saliba [14, 15] indicated that, due to the consolidation of hardened cement paste, concrete was strengthened under sustained loading so that measured fracture energy and strength increased slightly after a sustained loading is applied. However, the crack propagation during sustained loading was normally not considered in the determination of the fracture energy [14, 15], which may result in some deviations from the true value for the derived fracture energy from the fracture tests. Compared with the critical crack propagation length under the static loading, the crack propagation length after the creep under a high loading level could be different, which accordingly influences the determination of the unstable fracture toughness. Therefore, it is significantly important to study the crack propagation under high sustained loading so that the corresponding influence on the fracture properties of concrete, including the fracture energy and unstable fracture toughness, can be determined more accurately.

According to the fictitious crack model [16], there exists a fracture process zone (FPZ) ahead the microcracks, which characterises the strain softening and localisation behaviour through the relationship of the cohesive stress σ with the crack opening displacement w. Compared with the case under static loading, a decrease in the FPZ length, or a more brittle behaviour of concrete, could be observed in the creep fracture tests [12, 14]. This can also be explained by the development of microcracks under the creep, the prestressing in the upper zone of specimens [14], and the relaxation of the cohesive stress in the FPZ [12]. Due to the time-dependency of the fracture process zone, much attention has been paid to establishing an appropriate constitutive law to characterise the σ-w relationship. So far, three typical methods have been proposed to analyse time-dependent tension softening behaviour of concrete. The first one is based on the activation energy and loading rate dependent softening, which is appropriate when the effect of loading rate is significant [17]. The second one considers the viscosity characteristics of concrete materials by applying the rheological theory into the fictitious crack model [18, 19]. The third one combines the rheological theory with the micromechanical homogenisation to investigate the time-dependent tension softening behaviour in the FPZ [20, 21]. It should be mentioned that all three methods focus on the time-dependent σ-w relationships of the FPZ during the crack propagation process under sustained loading. Considering some concrete structures do not fail or initial cracks remain stable under sustained loading, the effects of sustained loading on the tension softening characteristics of the uncracked zone also need to be explored further. Therefore, to assess the load-carrying capacity of concrete structures under or after sustained loading, it is essentially important to establish the tension softening constitutive laws for concrete along the uncracked ligament.

Thus, the objective of this paper was to investigate the influence of different sustained loading levels on the fracture properties and tension softening constitutive law of concrete. Firstly, the basic creep tests were conducted under three-point bending (TPB) on the concrete beams at 30% of the peak load and also at the initial cracking load for 115 days. Thereafter, these specimens were unloaded from the creep frames and then subjected to TPB loading immediately until failure. Based on the experimental results of the TPB tests, a tension-softening constitutive law for the specimens after being subjected to sustained loading, i.e. creep, could be established by considering the effects of the microcracks which formed during the creep stage. Finally, the effect of sustained loading on the fractural parameters and tension-softening constitutive law could be explored by comparing with the results obtained from the static loading tests on the matured specimens.

2. Experimental Program

2.1 Preparation of the specimens

The dimensions of the concrete specimens for both basic creep tests and TPB tests were 500 mm × 100 mm × 100 mm (length × width × depth) with a 30-mm pre-notch. The mix proportions of the concrete were 1 : 0.60 : 2.01 : 3.74 (cement : water : sand : aggregate) by weight and the maximum coarse aggregate size was 10 mm. The specimens were demoulded 24 hours after casting and then cured in the standard curing room with 23°C and 90% relative humidity for three months to avoid possible early age autogenous shrinkage in the creep tests. The material properties of the concrete at the age of 28 days are listed in Table 1, where E, ρ, f_t and f_c denote the Young's modulus, density, splitting tensile and uniaxial compressive strength of concrete, respectively. In order to calibrate the applied load in the creep tests, three-point bending tests were performed to determine the peak load P_{max} on the pre-notched concrete beams, and the average value of P_{max} was determined as 3.81 kN at the age of 28 days.

Table 1 Material properties of concrete at the age of 28 days

Material property	E (GPa)	ρ (kg/m^3)	f_t (MPa)	f_c (MPa)
Quantity	32.9	2450	2.50	54.8

2.2 Creep tests

A steel loading frame was designed for performing the creep tests and the experimental set-up is illustrated in Fig.1. The load cell was connected onto a bolt and the load was applied by turning the bolt. The data acquisition system with a digital display was used to record the real-time load. The creep tests were conducted inside an environmental chamber with 23℃ and 60% relative humidity. To ensure only the basic creep to be measured in the tests, double-layer aluminium tape was utilised to seal the surfaces of the specimens to prevent the moisture evaporation.

Fig. 1. Set-up of the creep test

To investigate the creep behaviour at various loading levels, 30% of P_{max} and the initial cracking load were applied in the creep tests, respectively. For each load level, three specimens were adopted. For the specimens subjected to 30%P_{max}, the bolt was turned until the load level of 30% × 3.81 kN = 1.14 kN was reached. For the specimens subjected to the initial cracking load, four strain gauges were symmetrically put onto both sides of each specimen, 5 mm away from the tip of the pre-notch. Strain gauges were then connected to an Integrated Measurement & Control (IMC) dynamic date acquisition device. Once a new crack initiated, the measured strains from the strain gauges would drop rapidly due to the sudden release of the stored strain energy at the tip of the pre-crack [22]. Therefore, the initial cracking load could be obtained by gently turning the bolt until the measured strain values dropped quickly. The applied initial cracking loads for the three reference specimens were 2.85 kN, 2.95 kN and 2.97 kN, respectively. During the loading duration, the loads would be adjusted to the pre-set values if they descended by 2%, which caused the increase in the deformation over time. The loading point displacement (δ) and the crack mouth opening displacement (*CMOD*) were measured using dial gauges. In addition, three specimens, which were cast at the same time, were kept under the same conditions without loading, named as "aging specimens". The loading point displacement versus time curves of three specimens for two loading levels are shown in Fig. 2, where C-30 and C-ini denote the specimens loaded under 30%$P_{\max}$ and under the initial cracking load, respectively. After 115 days, the specimens in the creep tests were unloaded from the loading frames and then immediately subjected to the TPB tests.

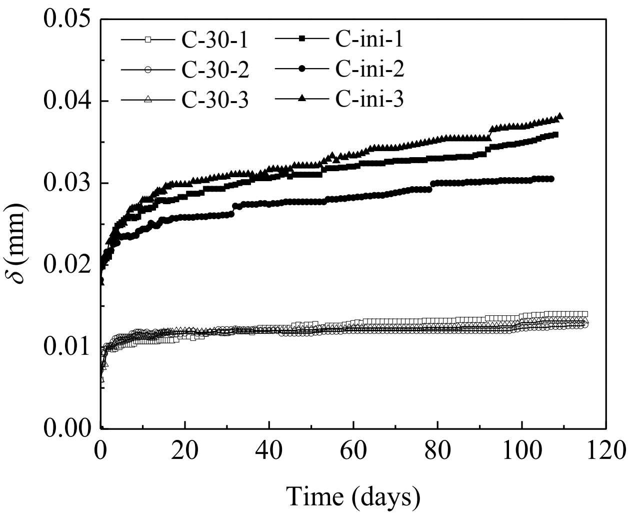

Fig. 2. Loading point displacement versus time curves in the creep tests

2.3 Three-point bending tests on the pre-notched beams

In order to investigate the effect of sustained loading on the fracture properties of concrete, the TPB tests were performed on the specimens which had been subjected to the creep testing in a 250 kN closed-loop servo MTS testing machine at a displacement rate of 0.048 mm/min. At the same time, the aging specimens were also tested to for comparing the experimental results after a sustained load with those under a static load. Two clip gauges were used to measure the CMOD, as shown in Fig. 3(a). In addition, to monitor the crack propagation length and crack tip opening displacement (CTOD), four clip gauges were placed equidistantly along the ligament length, as shown in Fig. 3(b).

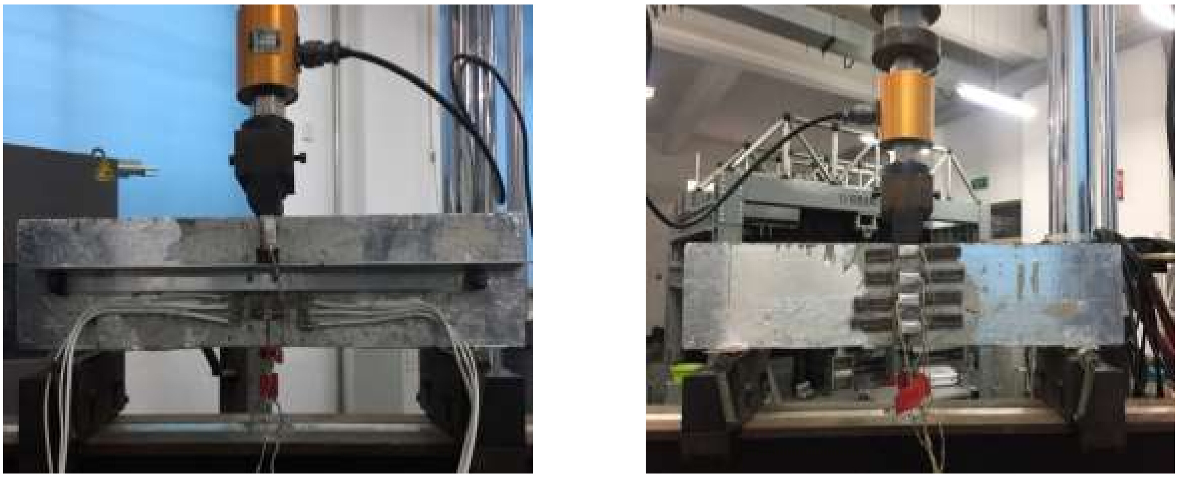

(a) Measuring loading point displacement and CMOD (b) Measuring CTOD

Fig. 3. Experimental set-up for the TPB tests after the creep testing

3. Test Results and Discussion

3.1 Effect of sustained loading on the crack propagation

From the load point displacement versus time curves in Fig. 2, it can be seen that for the specimens subjected to a sustained loading level of 30%P_{max}, the displacement increased rapidly in the early loading stage and gradually stabilised with the increase of time. In contrast, for the specimens subjected to a sustained loading level as the initial cracking load, the displacement continuously increased after the early loading stage, which confirms that the secondary creep occurred due to the crack propagation [1]. This indicates that the crack propagation occurred when the concrete specimens were subjected to the early sustained initial cracking load, while the crack would not propagate when the specimens were subjected to the sustained 30%P_{max} in the creep tests. In order to determine the crack propagation length during the creep tests, it is assumed that the creep displacements would recover when the specimens subjected to the creep testing were unloaded in the creep tests and then reloaded to the creep loading level in the subsequent TPB tests. Thus, the crack propagation length during the creep testing, a_f, can be derived from the TPB tests by measuring the *CMOD* and various crack opening displacements (*CODs)* along the ligament with four clip gauges as shown in Fig. 3(b). It should be noted that the COD can be employed to denote the opening displacement at any points of the crack surface, while the CMOD only denotes the crack opening displacement at the bottom of a beam.

The displacement at the crack initiation, w_{ini}, could be determined by measuring the *CTOD* with respect to the initial cracking load on the ageing specimens and was measured as 8.423 μm. According to the measured values of the *CMOD* and four *COD*s along the ligament, an approximately linear distribution of the crack opening displacements could be obtained, as shown in Fig. 4. Based on this relationship, the crack tip could be determined, with its displacement as w_{ini}. Accordingly, the crack propagation length could also be obtained from the position of the derived crack tip. The values of a_f for the C-ini series specimens are listed in Table 2. It can be seen that the average crack propagation length was determined as 13.50 mm, indicating a significant effect of sustained loading on the crack propagation. The same method was used to determine the critical crack length a_c (see Table 2), which was derived from the *COD*s corresponding to P_{max}. Meanwhile, to clarify the effect of sustained loading, the values of a_c which were obtained from the experimental investigations and calculated from Eq. (1) based on linear elastic fracture mechanics (LEFM) were compared (see Table 2)

$$a_c = \frac{2}{\pi}(D+H_0)\arctan\sqrt{\frac{B\cdot E\cdot CMOD_c}{32.6P_{max}} - 0.1135} - H_0 \quad (1)$$

where B and D are the width and depth of the TPB beam, $CMOD_c$ is the critical crack mouth opening displacement, and H_0 is the thickness of the knife edge and is equal to 3 mm in this study.

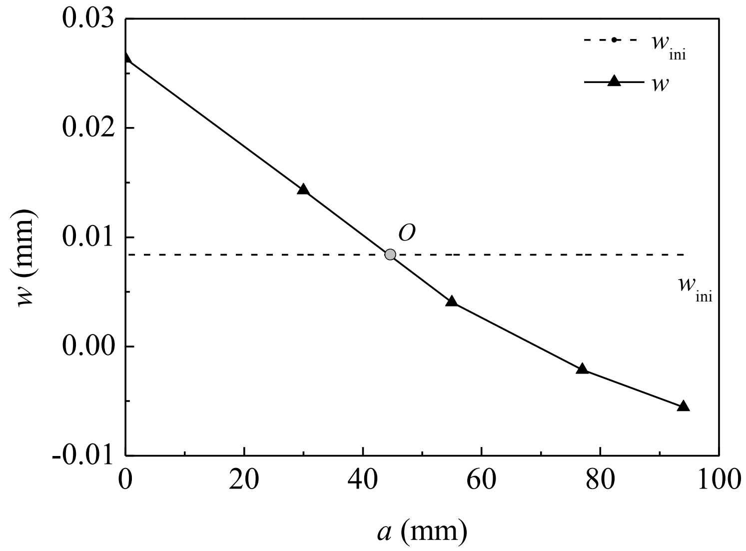

Fig. 4. Determination of the crack tip

Table 2. Experimental results for all specimens

Specimen	P_{ini} (kN)	$P_{\max}$ (kN)	a_{f} (mm)	a_{c} (mm)		$K_{\text{IC}}^{\text{un}}$ (MPa·m$^{1/2}$)	G_{f} (N/m)
				Exp.	Eq. (1)		
C-age-1	2.66	3.56	0	55.15	52.08	1.42	89.71
C-age-2	2.53	3.68	0	50.63	48.10	1.27	109.69
C-age-3	2.51	3.61	0	50.25	49.13	1.22	97.44
Mean value	2.55	3.59	0	52.01	49.77	1.28	98.95
C-30-1	2.88	3.79	0	52.78	50.98	1.31	98.22
C-30-2	2.61	3.25	0	54.90	54.36	1.29	93.93
Mean value	2.74	3.52	0	53.84	52.67	1.30	96.08
C-ini-1	--	3.69	13.04	60.54	51.18	1.79	89.31
C-ini-2	--	3.36	14.01	57.17	52.85	1.44	95.68
C-ini-3	--	3.37	13.40	57.69	53.81	1.47	113.73
Mean value	--	3.47	13.50	58.47	52.61	1.57	99.57

The results in Table 2 indicate that the values of a_{c} for the C-age series specimens obtained from the experiments and Eq. (1) are very close to each other, and this validates the test mothed in the current study for determining a_{c} using the clip gauges. The same case could be observed for the C-30 series specimens, indicating that low sustained loading, e.g. 30%$P_{\max}$, had almost no effect on

a_c. However, the scenario became different for the C-ini series specimens. The values of a_c obtained from the tests were larger than those derived from Eq. (1), indicating that Eq. (1) based on LEFM may not be appropriate for determining a_c if there is crack propagation during the creep stage. Due to the development of the cracks under the sustained loading, the critical crack lengths of the C-ini series specimens were larger than those for the aging specimens. Compared with the C-age series specimens, the newly expanded crack length was not very large, with the measured mean values of a_c for the C-age and C-ini series specimens as 22.01 mm and 14.97 mm, respectively.

3.2 Effect of sustained loading on the fracture properties

The *P-CMOD* curves of the three series concrete specimens are illustrated in Fig.5. For a vibrant comparison between the three loading conditions, the average curve was used for each loading condition. It can be seen from Fig. 5 that all the peak loads are very close for the specimens subjected to different sustained loadings and the aging specimens, and the mean values of P_{max} are 3.59 kN, 3.52 kN and 3.47kN for the C-age, C-30 and C-ini series specimens, respectively. The peak load P_{max} seemed not to be largely affected by the sustained loading applied in this study. Similar conclusions were also drawn by other researchers [11, 12]. After obtaining the peak loads and the critical crack propagation lengths from the tests, the unstable fracture toughness K_{IC}^{un} can be calculated using Eq. (2) as [23], where S is the span of the beam and is equalled to 400 mm in this study

$$K_{IC}^{un} = \frac{3P_{max}S}{2D^2B}\sqrt{a_c}F_2\left(\frac{a_c}{D}\right) \quad (2)$$

with $F_2\left(\frac{a_c}{D}\right)$ to be calculated using Eq. (3) as

$$F_2\left(\frac{a}{D}\right)=\frac{1.99-\left(\frac{a}{D}\right)\left(1-\frac{a}{D}\right)\left[2.15-3.93\left(\frac{a}{D}\right)+2.7\left(\frac{a}{D}\right)^2\right]}{\left(1+2\frac{a}{D}\right)\left(1-\frac{a}{D}\right)} \tag{3}$$

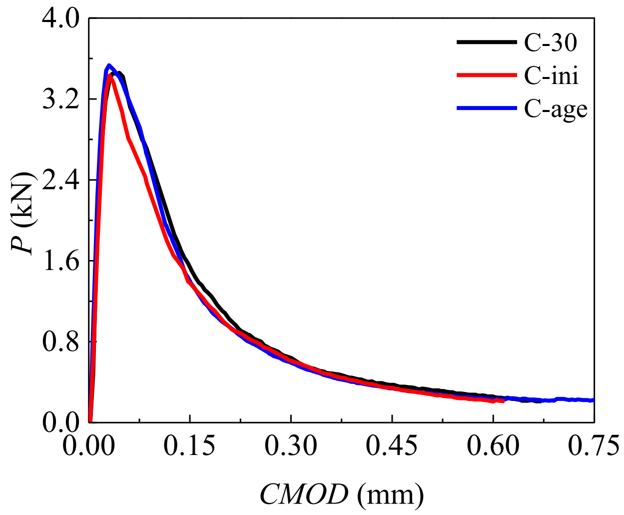

Fig. 5 Average *P-CMOD* curves for three series specimens

Considering the effects of sustained loading on the fracture properties of concrete, the values of a_c from Eq. (1) might not be appropriate to be used to calculate K_{IC}^{un}. Alternatively, the obtained values of a_c from the experiment were adopted for calculating K_{IC}^{un}, as listed in Table 2. It can be seen that there was a very small difference in K_{IC}^{un} between the C-age and C-30 series specimens. However, the mean value of K_{IC}^{un} for the C-ini series specimens increased by 22.7% compared with that for the C-age series specimens. In particular, the mean value of P_{max} for the C-ini series specimens was smaller than that for the C-age series specimens. This indicates that the low sustained loading did not largely influent the unstable fracture toughness. However, the unstable fracture toughness significantly increased under the high sustained loading, due to the larger critical crack propagation length compared with that under the static loading condition.

Besides the unstable fracture toughness, the fracture energy G_f is also an important fracture parameter for concrete and is defined as the required energy for creating the cracking area. It can be calculated using Eq. (4) as [24]

$$G_{\rm f}=\frac{W_{\rm f}}{A_{\rm lig}}=\frac{W_0+2mg\delta_0}{B(D-a_0)} \tag{4}$$

where $W_{\rm f}$ is the total absorbed energy, $A_{\rm lig}$ is the area of ligament, W_0 is the area below the measured load-deformation curve, mg is the self-weight of the beam, δ_0 is the loading-point displacement at failure, and a_0 is the initial crack length.

For the C-age and C-30 series specimens, there were no crack propagations during the creep testing stage, so that the ligament areas did not change and their fracture energies still could be calculated using Eq. (4). In contrast, for the C-ini series specimens, the ligament areas decreased because the new cracks formed during the creep testing stage. In order to evaluate the effect of these new cracks on the fracture energy, the total energy can be divided into two parts, i.e. the energy dissipated during the creep stage, $W_{\rm c}$, and the energy dissipated in the subsequent static TPB test, $W_{\rm f}$. The combination of $W_{\rm c}$ and $W_{\rm f}$ governs the complete crack propagation, as illustrated in Fig. 6. Hence, the equation for the fracture energy can be revised as

$$G_{\rm f}=\frac{W_{\rm f}+W_{\rm c}}{A_{\rm lig}}=\frac{W_0+2mg(\delta_0+\delta_{\rm c})+W_{\rm c}}{B(D-a_0)} \tag{5}$$

where $\delta_{\rm c}$ is the residual displacement in the creep tests.

The calculated $G_{\rm f}$ values using Eq. (4) for the C-age and C-30 series specimens, and Eq. (5) for the C-30 series specimens are all listed in Table 2. It can be seen that, compared with the aging specimens, the sustained loading has slight effect on the fracture energy through the energy dissipated during the creep testing stage. The cohesive stresses were transferred in the FPZ and the energy was dissipated, so that the fracture energy could be directly related to the FPZ evolution. Microscopically, there were no micro-defects, i.e. no micro-cracks or weak planes formed around aggregates under the low sustained loading. In this case, the FPZ evolution should be the same as that under the static loading. In contrast, the micro-cracks would initiate under the high sustained loading, resulting in the slow extension of the FPZ and variations of the crack-bridging stress area. However, the sustained load level applied at the crack initiation in this study was not high enough.

According to the comparison of the a_c values for the C-age and C-ini series specimens in Table 2, no significant increase was observed. Since the experimental results confirmed that the fracture energy did not change with the sustained load levels, this indicated that the width or height of the FPZ was not affected by the sustained loads applied in this study.

Meanwhile, the mean values of W_f and W_c for the C-ini series specimens were determined as 54.75 N·m and 571.7 N·m, respectively, giving the ratio of W_c/W_f as 9.6%. Therefore, the fracture energy would be underestimated if the LEFM is adopted without considering the crack development during the creep testing stage.

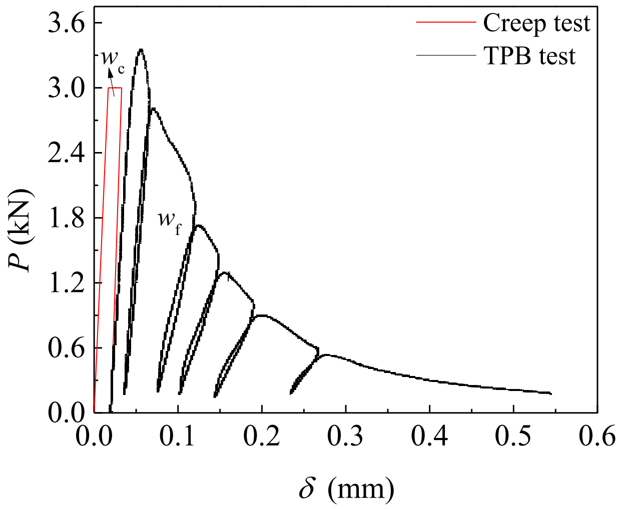

Fig. 6. Load-displacement curves in the creep and static TPB tests

3.3 Effect of sustained loading on the tension-softening constitutive law

The modified J-integral method proposed by Niwa [25] was utilised in this study to investigate the tension-softening constitutive law of concrete after being subjected to the sustained loading. This method has been used to evaluate the tension-softening relationships for polymer cement mortar-concrete [26] and rock-concrete interface [27]. The J-integral is defined as the energy available for crack propagation, $E(\delta)$, which can be interpreted as the total absorbed energy of a cracked specimen minus the released elastic energy during unloading process. If both the unloading and reloading paths can be assumed as linear, $E(\delta)$ can be written as

$$E\left(\delta\right)=\int_{0}^{\delta}P(\delta)\,d\delta-\frac{1}{2}P\left(\delta\right)\left(\delta-\delta_{\mathrm{P}}\right) \tag{6}$$

where δ is the displacement for a load P, and δ_{p} is the residual displacement for a linear unloading-reloading process from the descending branch of the P-δ curve, see Fig. 7.

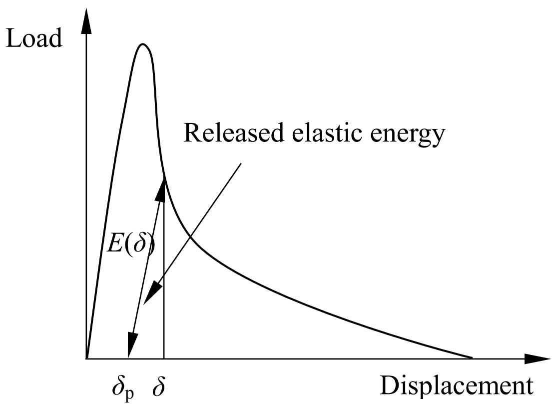

Fig. 7. Illustration of the Modified J integral method

It should be noted that Eq. (6) is only applicable for the specimens without microcracks existing at their pre-crack tips, i.e. the C-age and C-30 series specimens. For the C-ini series specimens, propagations of the microcracks were observed in the creep tests, so that the energy dissipations caused by the microcracks should be considered. Therefore, the cohesive stress $\sigma(w)$ is applied on the FPZ by introducing a tension-softening relationship derived from the test results on the C-age series specimens. Meanwhile, a reduction factor of 0.8 was used to consider the effect of the cohesive stress relaxation [6]. The energy dissipation for the C-ini series specimens includes two parts: one part is for overcoming the effect of the cohesive stress along the microcrack length a_{f}, and another part is for forming the new cracks. Therefore, Eq. (6) for the energy balance can be rewritten as

$$E(\delta)=\int_{0}^{\delta}P(\delta)d\delta-\frac{1}{2}P(\delta)(\delta-\delta_{\mathrm{p}})-0.8E(\sigma) \tag{7}$$

with $E(\sigma)$ as the energy caused by the cohesive stress along a_{f} which can be obtained from

$$E(\sigma) = B\int_0^{a_f}\int_{w_1(x)}^{w_2(x)} \sigma(w)dw\,dx + B\int_0^{a_f} \frac{1}{2}\sigma(w_p)(w_p - w_c)dx \tag{8}$$

where σ is the cohesive stress acting on the fracture process zone, w is the crack width, x is the distance from the pre-crack tip, w_p is the *CTOD* before unloading in the creep test, w_c is the residual *CTOD* after unloading in the creep test, $w_1(x) = \frac{x}{a_f}w_p$, $w_2(x) = \frac{(a-x)}{a}w$, and a is the crack length. The first term in Eq. (8) denotes the energy caused by the cohesive stress when the applied load in the static TPB test is larger than the sustained loading in the creep test, while the second term denotes the energy when the applied load in the static TPB test is smaller than the sustained loading in the creep test.

From the experimental results, the mean values of w_p, w_c and a_f for the C-ini series specimens were obtained as 13.86 μm, 4.78 μm and 13.5 mm, respectively. Thus, the tension-softening constitutive law can be determined by establishing the relationships between the crack propagation length a, the loading-point displacement δ and the crack opening displacement w.

Fig. 8 illustrates the P-δ curves for Specimens C-age-1 and C-ini-1 during the complete crack propagation. Based on the unloading-reloading circles in the tests, the δ_p-δ relationship can be derived by normalising δ_p to the maximum displacement δ_{max} as (Fig. 9)

$$\delta_p / \delta_{max} = (\delta / \delta_{max})^{\eta} \tag{9}$$

where η is an empirical coefficient and is obtained by statistically fitting the test results as 1.26, 1.37, 1.35 for the C-age, C-30 and C-ini series specimens, respectively.

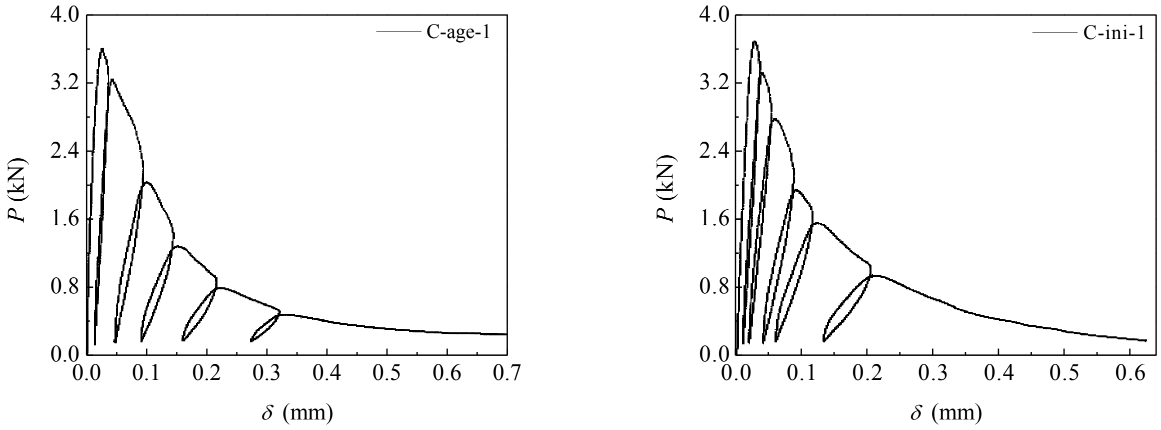

(a) C-age-1 (b) C-ini-1

Fig. 8. Load-displacement curves for different specimens

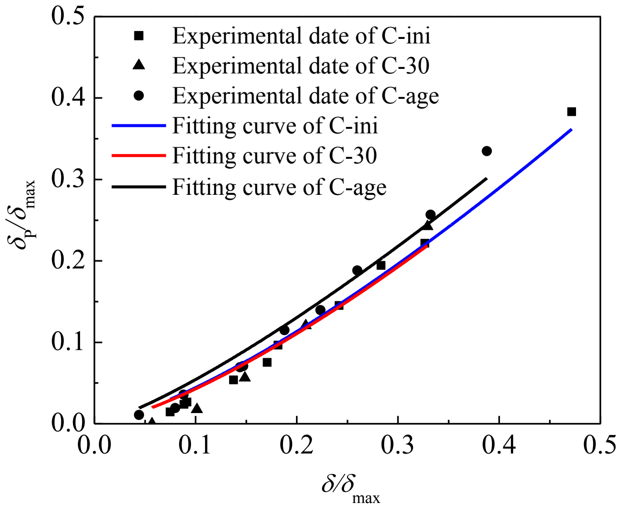

Fig. 9. Relationships between δ_p / δ_{max} and δ / δ_{max} for different specimens

If the energy $E(\delta)$ is used to drive the new crack propagation, the tension-softening relationship can be derived as

$$\sigma(w) = \frac{1}{\Delta a \cdot B}\left[2E^{'}(w) + wE^{''}(w)\right] \tag{10}$$

where $E'(w)$ and $E''(w)$ are the first and second derivatives of the energy $E(w)$. The crack widths at the four equally divided points of the ligament can be measured by using four clip gauges (see Fig. 3(b)). Meanwhile, the crack propagation length Δa can be derived by measuring the fictitious crack tip, as illustrated in Fig. 4. Based on the experimental results, the Δa-w relationship (normalized by dividing the ligament height $a_{\max}$ and the maximum crack width $w_{\max}$) and the Δa-δ relationship (normalized by dividing $a_{\max}$ and the maximum displacement $\delta_{\max}$) can be obtained as follows

$$\Delta a / a_{\max} = 1 - \left(1 - \sqrt{w / w_{\max}}\right)^{\gamma} \tag{11}$$

$$\Delta a / a_{\max} = 1 - \left(1 - \sqrt{\delta / \delta_{\max}}\right)^{\kappa} \tag{12}$$

where γ and κ empirical constants and are obtained by statistically fitting the test results as $\gamma = 3.11$, 3.63, 2.40 and $\kappa = 2.92$, 3.20, 2.00 for the C-age, C-30 and C-ini series specimens, respectively. Figs. 10(a) and (b) illustrate the experimental results and the fitting curves of $\Delta a/a_{\max}$ versus $w/w_{\max}$ and $\Delta a/a_{\max}$ versus $\delta/\delta_{\max}$ for the C-ini series specimens.

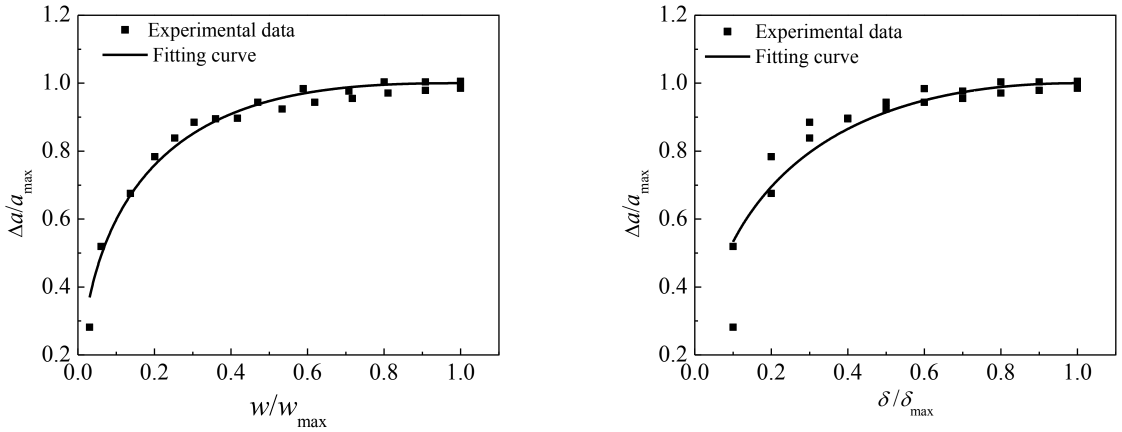

(a) $\Delta a/a_{\max}$ versus $w/w_{\max}$ (b) $\Delta a/a_{\max}$ versus $\delta/\delta_{\max}$

Fig. 10. $\Delta a/a_{\max}$ versus $w/w_{\max}$ and $\Delta a/a_{\max}$ versus $\delta/\delta_{\max}$ relationships for the C-ini specimens

Finally, an exponential expression for the tension-softening constitutive law can be obtained by substituting Eqs. (9), (11) and (12) into Eq. (8) (also normalized by dividing f_t and w_0) as

$$\sigma(w) = f_{\mathrm{t}} \left[\left(1 + \frac{c_1^3}{w_0^3} w^3\right) e^{-\frac{c_2}{w_0} w} - \frac{(1 + c_1^3) e^{-c_2}}{w_0} w \right] \tag{13}$$

where c_1 and c_2 are empirical constants. The experimental results indicates that the derived tension softening constitutive laws for the C-age and C-30 series specimens were close to each other, with

$c_1 = 3$, $c_2 = 7$ and $w_0 = 0.18$ mm obtained. In contrast, for the C-ini series specimens, $c_1 = 3$, $c_2 = 6$ and $w_0 = 0.15$ mm were obtained. Furthermore, for practical applications, a bilinear relationship based on the following four parameters, f_t, σ_s, w_s and w_0, can be derived to represent the real tension-softening constitutive law. Once the break-point with the coordinates (σ_s, w_s) is determined, the exponential tension-softening constitutive law can be transformed to the bilinear law by enforcing the same fracture energy G_f. Using the method proposed by Wittmann et al [28], the parameters for the bilinear expression of the tension-softening constitutive law are given as follows

$$\sigma_s = 0.15 f_t \tag{14}$$

$$w_s = \alpha\, G_f / f_t \tag{15}$$

$$w_0 = \beta\, G_f / f_t \tag{16}$$

where α and β are empirical constants. For the C-age and C-30 series specimens, $\alpha = 1.2$ and $\beta = 5$, while for the C-ini series specimens, $\alpha = 1.4$ and $\beta = 4$.

Fig. 11 illustrates the exponential and bilinear relationships of σ-w for different series specimens. It can be seen that the simplified bilinear relationship is a reasonable approximation of the exponential one, and can reflect the characteristic of the real σ-w relationship while a bilinear tension softening constitutive law is more conveniently employed for practical design with much less computational cost. In addition, based on the derived bilinear σ-w relationships illustrated in Fig. 11(d), the softening constitutive laws under various conditions show obvious differences. The σ-w relationship for the specimens under low load level, i.e. the C-30 series specimens, is similar to the one for the specimens tested in a static condition, i.e. the C-age series specimens. This indicates that the low load level has little influence on the tension-softening constitutive law. However, the scenario is different in the case of high load level. Compared with the static condition, the COD at the breaking point, w_s, increased from $1.2G_f/f_t$ to $1.4G_f/f_t$ and the free-stress COD, w_0, decreased from $5G_f/f_t$ to $4G_f/f_t$ under the high load level. With the increasing sustained load level, the aggregate interlocking effects would be weakened and the frictional sliding effects among the aggregates would increase over time. Accordingly, compared with the case under static loading, the transference of the cohesive stress in the FPZ would decrease even with the same crack opening displacement under the sustained loading. Therefore, the free-stress crack opening displacement w_0 would decrease with the increasing sustained load level. Meanwhile, according to the experimental measurements, the fracture energy would not be affected significantly by the sustained loading applied in this study. To ensure the energy balance, w_s would decrease with the increasing w_0. In summary, this indicates that, under a sustained high load level, a shorter FPZ length could be formed, resulting in the increase in the brittleness of concrete.

It should be noted that, according the size effect law [29, 30], the variation of fracture energy was a function of the specimen size and shape. In addition, based on the boundary size model [31, 32], the fracture energy decreased as the crack tip was close to the top surface of a specimen. In this study, the size effect of the fracture energy was not considered when deriving the tensile softening relationship.

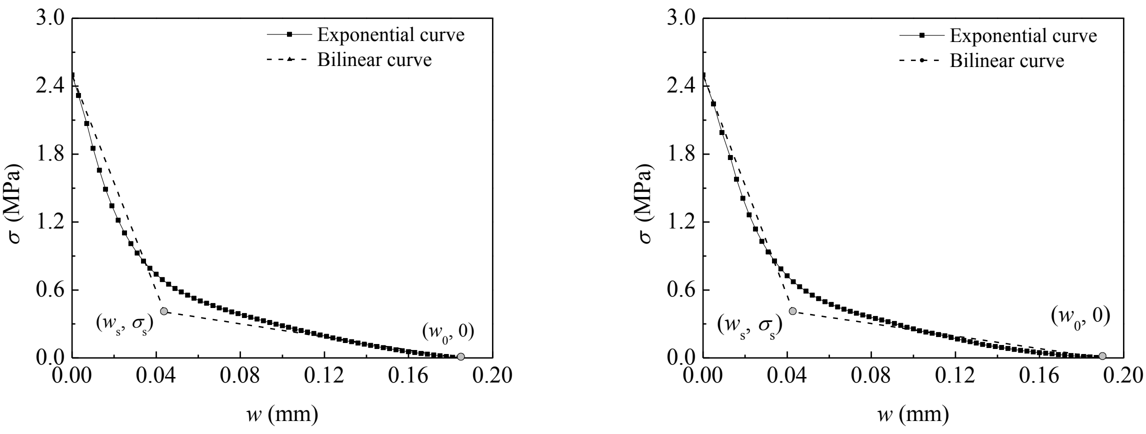

(a) Specimen C-age-1 (b) Specimen C-30-1

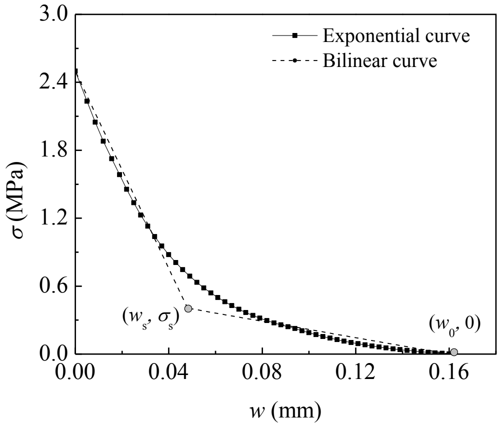

(c) Specimen C-ini-1

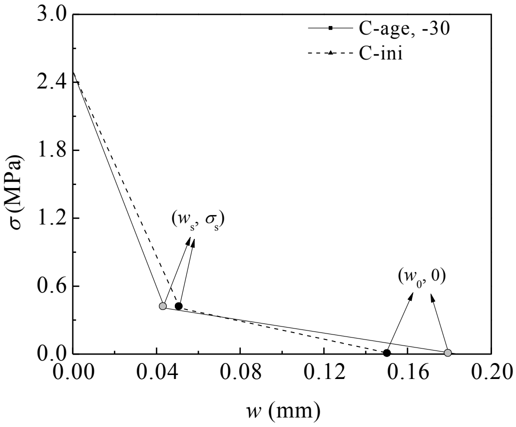

(d) Comparison of bilinear relationships

Fig. 11. Exponential and bilinear σ-w relationships

4. Conclusions

The creep tests were conducted on the concrete specimens for a duration of 115 days by applying the sustained loading levels of 30%$P_{\max}$ and the initial cracking loads. Thereafter, these specimens were tested under the static TPB. By comparing the critical crack length, the unstable fracture toughness and the fracture energy from the specimens subjected to the creep loading and the aging specimens, the influences of the sustained loading on the fracture properties of concrete were extensively examined. Based on the experimental results, the tension-softening constitutive laws for those TPB specimens were derived using the modified J-integral method. According to the experimental and theoretical studies, the following conclusions can be drawn:

1. For low sustained loading levels, e.g. 30%$P_{\max}$, no crack propagations were observed in the creep tests. Accordingly, the low sustained loading had no effects on the fracture properties of concrete, including the fracture energy, the critical crack length, the initial and unstable fracture toughnesses, and the tension-softening constitutive law. Therefore, the fracture parameters measured from the static loading tests can be utilized to assess the fracture characteristics of concrete subjected to low sustained loading.
2. For high sustained loading levels, e.g. the initial crack load, the crack propagation length was

measured as 13.5 mm on average in the creep tests. Compared with the aging specimens, the critical crack length and the unstable fracture toughness increased for the specimens subjected to the high sustained loading. However, the effect of the high sustained loading on the fracture energy becomes insignificant if considering the crack propagation in the creep stage. In contrast, the fracture energy could be underestimated from the results based on LEFM without considering the developed crack in the creep stage.

3. By introducing the cohesive stress on the creep-induced microcracks into the modified J-integral method, the tension-softening constitutive law for the specimens subjected to the creep tests at a high sustained loading level was obtained. For practical applications, the tension-softening constitutive expression was simplified as a bilinear form. Compared with the aging specimens in the static TPB tests, the COD at the breaking point, w_s, increased from $1.2G_f/f_t$ to $1.4G_f/f_t$, while the free-stress COD, w_0, decreased from $5G_f/f_t$ to $4G_f/f_t$ under the high sustained loading level. Consequently, a shorter FPZ length could be expected, resulting in the increase in the brittleness of concrete.

Acknowledgments

The authors gratefully acknowledge the financial support of the National Natural Science Foundation of China under the grants of NSFC 51478083, NSFC 51421064 and NSFC 51109026, the Natural Science Foundation of Liaoning Province of China under the grant of 20170540183, and the National Basic Research Program of China (The 973 Program) under the grant of 2015CB057703.

References

[1] Rossi P, Boulay C, Tailhan JL, Martin E, Desnoyers D. Macrocrack propagation in concrete specimens under sustained loading: Study of the physical mechanisms. Cement Concrete Res 2014;63:98-104.

[2] Karihaloo BL, Santhikumar S. Application of a visco-elastic tension-softening constitutive model to cracked and ageing concrete. Constr Build Mater 1999;13:15-21.

[3] Zhou FP. Time-dependent crack growth and fracture in concrete.: Lund University of Technology. Lund, Sweden; 1992.
[4] Bažant ZP. Current status and advances in the theory of creep and interaction with fracture. In: Proceedings of the 5th International RILEM Symposium on Creep and Shrinkage of Concrete. Barcelona, Spain; 1993.
[5] Bažant ZP, Gettu R. Rate effects and load relaxation in static fracture of concrete. ACI Mater J 1992;89:456-68.
[6] Bažant ZP, Li YN. Cohesive crack with rate-dependent opening and viscoelasticity: I. Mathematical model and scaling. Int J Fracture 1997;86:247-65.
[7] Sarkhosh R, Walraven J, Den Uijl J. Time-dependent behavior of cracked concrete beams under sustained loading. In: Proceedings of the 8th International Conference on Fracture Mechanics of Concrete and Concrete Structures. Toledo, Spain; 2013.
[8] Chaimoon K, Attard MM, Tin-Loi F. Crack propagation due to time-dependent creep in quasi-brittle materials under sustained loading. Comput Method Appl M 2008;197:1938-52.
[9] Tailhan JL, Boulay C, Rossi P, Le Maou F, Martin E. Compressive, tensile and bending basic creep behaviours related to the same concrete. Struct Concrete 2013;14:124-30.
[10] Barpi F, Valente S. Failure lifetime of concrete structures under creep and fracture. Mag Concrete Res 2011;63:371-6.
[11] Omar M, Haidar K, Loukili A, Pijaudier-Cabot G. Creep load influence on the residual capacity of concrete structure: Experimental investigation. In: The 5th International Conference on Fracture Mechanics of Concrete and Concrete Structures. Vail, United States; 2004.
[12] Omar M, Loukili A, Pijaudier-Cabot G, Pape YL. Creep-damage coupled effects: Experimental investigation on bending beams with various sizes. J Mater Civil Eng 2009;21:65-72.
[13] Carpinteri A, Valente S, Zhou F, Ferrara G, Melchiorri G. Tensile and flexural creep rupture tests on partially-damaged concrete specimens. Mater Struct 1997;30:269-76.
[14] Saliba J, Loukili A, Grondin F, Regoin J. Experimental study of creep-damage coupling in concrete by acoustic emission technique. Mater Struct 2012;45:1389-401.
[15] Saliba J, Grondin F, Loukili A, Regoin J. Coupling creep and damage in concrete under high sustained loading. In: Proceedings of The 7th International Conference on Fracture Mechanics of Concrete and Concrete Structures. Jeju, Korea; 2010.
[16] Hillerborg A, Modéer M, Petersson PE. Analysis of crack formation and crack growth in concrete by means of fracture mechanics and finite elements. Cement Concrete Res 1976;6:773-81.
[17] Bažant ZP. Creep and damage in concrete. In: Proceedings of The 4th Materials Science of Concrete. Westerville, Ohio; 1995.
[18] Hansen E. A visco-elastic fictitious crack model. In: Proceedings of Micromechanics of Quasi-brittle Materials. London; 1992.
[19] Carpinteri A, Valente S, Zhou F, Ferrara G, Melchiorri G. Crack propagation in concrete specimens subjected to sustained loads. In: Fracture Mechanics of Concrete Structures. Aedificatio, Freiburg; 1995.
[20] Barpi F, Valente S. Creep and fracture in concrete: a fractional order rate approach. Eng Fract Mech 2002;70:611-23.
[21] Barpi F, Valente S. A fractional order rate approach for modeling concrete structures subjected to creep and fracture. Int J Solids Struct 2004;41:2607-21.
[22] Dong W, Wu ZM, Zhou XM. Calculating crack extension resistance of concrete based on a new crack propagation criterion. Constr Build Mater 2013;38:879-89.

[23] Xu SL, Reinhardt HW. Determination of double-K criterion for crack propagation in quasi-brittle fracture, Part II: Analytical evaluating and practical measuring methods for three-point bending notched beams. Int J Fracture 1999;98:151-77.
[24] Petersson PE. Crack growth and development of fracture zones in plain concrete and similar materials. Lund University of Technology. Lund, Sweden; 1981.
[25] Niwa J, Sumranwanich T, Tangtermsirikul S. New method to determine tension softening curve of concrete. In: Fracture Mechanics of Concrete Structures Proceedings FRAMCOS-3. Freiburg, Germany; 1998.
[26] Zhang DW, Ueda T, Furuuchi H. Fracture mechanisms of polymer cement mortar: Concrete interfaces. J Eng Mech 2012;139:167-76.
[27] Dong W, Wu ZM, Zhou XM. Fracture mechanisms of rock-concrete interface: Experimental and numerical. J Eng Mech 2016;142:04016040.
[28] Wittmann F, Rokugo K, Brühwiler E, Mihashi H, Simonin P. Fracture energy and strain softening of concrete as determined by means of compact tension specimens. Mater Struct 1988;21:21-32.
[29] Bažant ZP, Kazemi MT. Determination of fracture energy, process zone length and brittleness number from size effect, with application to rock and concrete. Int J Fracture 1990; 44:111-131.
[30] Hoover CG, Bažant ZP. Universal size-shape effect law based on comprehensive concrete fracture tests. J Eng Mech 2014; 140(3):473-479.
[31] Hu XZ. Fracture energy and fracture process zone. Mater Struct 1992; 25:319-326.
[32] Hu XZ, Guan JF, Wang YS, Keating A and Yang ST. Comparison of boundary and size effect models based on new developments. Eng Fract Mech 2017;175:146-167.